Journal of Biomedical Optics

SPIEDigitalLibrary.org/jbo

Investigation of lipid homeostasis in living *Drosophila* by coherent anti-Stokes Raman scattering microscopy

Cheng-Hao Chien
Wei-Wen Chen
June-Tai Wu
Ta-Chau Chang

SPIE

Investigation of lipid homeostasis in living *Drosophila* by coherent anti-Stokes Raman scattering microscopy

Cheng-Hao Chien,[a,b] Wei-Wen Chen,[b,c,d] June-Tai Wu,[e,f] and Ta-Chau Chang[a,b,c]
[a]National Yang-Ming University, Institute of Biophotonics, Taipei 112, Taiwan
[b]Institute of Atomic and Molecular Sciences, Academia Sinica, Taipei 106, Taiwan
[c]Institute of Atomic and Molecular Sciences, Molecular Science and Technology Program, Taiwan International Graduate Program, Academia Sinica, Taipei 106, Taiwan
[d]National Tsing Hua University, Department of Chemistry, Hsinchu 30013, Taiwan
[e]National Taiwan University, Institute of Molecular Medicine, College of Medicine, Taipei 100, Taiwan
[f]National Taiwan University Hospital, Department of Medical Research, Taipei 100, Taiwan

Abstract. To improve our understanding of lipid metabolism, *Drosophila* is used as a model animal, and its lipid homeostasis is monitored by coherent anti-Stokes Raman scattering microscopy. We are able to achieve *in vivo* imaging of larval fat body (analogous to adipose tissue in mammals) and oenocytes (analogous to hepatocytes) in *Drosophila* larvae at subcellular level without any labeling. By overexpressing two lipid regulatory proteins—Brummer lipase (Bmm) and lipid storage droplet-2 (Lsd-2)—we found different phenotypes and responses under fed and starved conditions. Comparing with the control larva, we observed more lipid droplet accumulation by ~twofold in oenocytes of fat-body-Bmm-overexpressing (FB-Bmm-overexpressing) mutant under fed condition, and less lipid by ~fourfold in oenocytes of fat-body-Lsd-2-overexpressing (FB-Lsd-2-overexpressing) mutant under starved condition. Moreover, together with reduced size of lipid droplets, the lipid content in the fat body of FB-Bmm-overexpressing mutant decreases much faster than that of the control and FB-Lsd-2-overexpressing mutant during starvation. From long-term starvation assay, we found FB-Bmm-overexpressing mutant has a shorter lifespan, which can be attributed to faster consumption of lipid in its fat body. Our results demonstrate *in vivo* observations of direct influences of Bmm and Lsd-2 on lipid homeostasis in *Drosophila* larvae. [DOI: 10.1117/1.JBO.17.12.126001]

Keywords: *drosophila*; lipid metabolism; coherent anti-Stokes Raman scattering microscopy; two-photon excitation fluorescence microscopy; fat body; oenocyte; *in vivo*; label-free.

Paper 12627P received Sep. 21, 2012; revised manuscript received Nov. 9, 2012; accepted for publication Nov. 12, 2012; published online Dec. 3, 2012.

1 Introduction

Complex organisms require proper coordination of energy metabolism to cope with environmental conditions. Since lipid serves as an important source of energy, lipid regulation plays a critical role during fluctuation of food availability. This involves coordination of several organs such as the central nervous system, adipose tissue, and liver, as well as metabolic modulation between lipid expenditure and storage.[1] It is known that imbalance of lipid metabolism lead to many diseases including obesity and diabetes.[2] Understanding of lipid regulation in organisms can help us find the solution to these problems.

Drosophila, one of the most valuable model animals, is a good candidate for the studies of lipid metabolism.[3–5] *Drosophila* mainly stores neutral lipid in the fat body, a specialized organ analogous to the adipose tissue in mammals. The fat body supplies essential energy during larval development and is involved in lipid metabolism and hormone production.[6] When the food is deprived, lipid is released from the fat body and then processed in another specialized cell called oenocyte, analogous to the hepatocyte in mammals.[7] Larval oenocytes communicate with the fat body to perform lipid regulation and accumulate lipid during starvation. Many orthologues of human lipid-metabolizing genes are specifically expressed in oenocytes.[7] Considering the conservation and similarity between *Drosophila* and humans, the fat body and oenocytes in *Drosophila* provide a suitable platform in modeling human lipid metabolism and metabolic disease.[7,8]

The PAT (Perilipin, ADRP, and TIP47) family of lipid-droplet-associated proteins are key players in lipid metabolic pathways and have five members in mammals: PERILIPIN1, PERILIPIN2, . . . , PERILIPIN5.[9,10] In *Drosophila*, the genetic homolog of mammalian PERILIPIN1 and PERILIPIN2 are lipid storage droplet-1(Lsd-1) and Lipid storage droplet-2 (Lsd-2).[11–15] Lsd-2 localizes at the surface of *Drosophila* lipid droplets (LDs) and participates in normal lipid storage.[12] Overexpression of Lsd-2 in the fat body results in higher triacylglycerol (TAG) level and obesity phenotype in adult flies, and these obese flies are more resistant to starvation than control wild-type flies.[12] On the other hand, the Brummer lipase (Bmm), which is the homolog of mammalian adipocyte triglyceride lipase (ATGL), promotes lipolysis and lipid mobilization in LDs.[16] Overexpression of Bmm in the fat body decreases TAG content in adult flies. Lsd-2 and Bmm act in an antagonistic manner to regulate the balance between lipid storage and lipolysis in LDs.[16]

Conventionally, people use stains like Oil Red O[7] to visualize LDs in *Drosophila*. However, it requires careful fixation and

Address all correspondence to: Ta-Chau Chang, National Yang-Ming University, Institute of Biophotonics, Taipei 112, Taiwan. Tel: +886-2-23668231; Fax: +886-2-23620200; E-mail: tcchang@po.iams.sinica.edu.tw

0091-3286/2012/$25.00 © 2012 SPIE

staining procedures and is restricted to fixed tissues or cells, which is not applicable for live imaging. Although there are some vital dyes such as Nile Red and BODIPY for neutral lipid imaging in living cells,[17,18] their accuracy for *in vivo* lipid imaging is still questionable.[19,20] For *in vivo* imaging, people usually label fluorescent fusion proteins specifically on the surface of LDs.[21] In addition to the well-developed genetic modulation methods and biochemical assays, the advances of imaging techniques allow us to visualize neutral lipid in living *Drosophila* without any labeling.[22–26] One of them is coherent anti-Stokes Raman scattering (CARS) microscopy.[25]

Because CARS is much stronger than conventional Raman scattering, it is more applicable to form image contrast of vibrational modes in microscopy without the need of fluorescence.[27] CARS microscopy was first reported in 1982[28] and became popular after 1999 with the adoption of advanced lasers and collinear optical design.[29] Because of high density of C-H bond in lipid molecules, it is often used for lipid imaging without labeling in biomedical researches. CARS microscopy has been applied to analysis of tissues/organs from mouse,[30–37] human,[38–40] and for *in vivo* imaging of model animals such as *C. elegans*,[20,41,42] zebrafish,[43] and *Drosophila*.[25,44]

By combining two-photon excitation fluorescence (TPE-F) microscopy, we have acquired lipid and autofluorescence imaging in living *Drosophila* and observed fat body remodeling process during metamorphosis[25] and lipid accumulation in oenocytes.[44] To further study lipid homeostasis in *Drosophila*, here we monitored LDs in both larval oenocytes and fat body of living larvae under fed and starved conditions. We analyzed the lipid content and size of LDs in oenocytes as well as in the fat body from CARS/TPE-F images. Compared with control larvae, mutants that overexpress Bmm or Lsd-2 in the fat body show significant difference of lipid content in oenocytes and fat body both under fed and starved conditions, revealing the characteristic in their lipid metabolism. In addition, we examined their larval viability during long-term starvation and found the correlation with their consumption of lipid in the fat body. Through *in vivo* observations, our findings characterize the effects of metabolic imbalance in *Drosophila* larvae.

2 Materials and Methods

2.1 *Drosophila*

w^{1118} strain was provided by fly core facility in College of Medicine, National Taiwan University. FB-Gal4, UAS-Bmm, and UAS-Lsd-2 strains were kindly provided by Dr. Ronald Kühnlein.[12,16] To overexpress Bmm or Lsd-2 in the fat body, we crossed FB-Gal4 with UAS-Bmm or UAS-Lsd-2 to generate FB-Gal4:UAS-Bmm (FB-Bmm-overexpressing mutant) and FB-Gal4:UAS-Lsd-2 (FB-Lsd-2-overexpressing mutant), respectively. The w^{1118} and FB-Gal4 strains were used as the controls in oenocyte and fat body experiments, respectively. All strains were raised at 22°C using a standard agar diet (1% autolyzed yeast, 5.8% cornmeal, 5% glucose, 0.6% agar).

2.2 *Oil Red O Staining*

The procedure for staining *Drosophila* larval oenocytes and fat body is described as follows: larvae were carefully dissected in phosphate buffered saline (PBS) and fixed in 4% paraformaldehyde for 25 (oenocyte) or 10 min (fat body). Specimens were then rinsed with distilled water and incubated in Oil Red O stain for 20 min. (Saturated Oil Red O in isopropanol/water = 1:1 solution. Oil Red O was from Sigma-Aldrich, UK.) After staining, the specimens were rinsed with distilled water and ready for imaging by bright field microscopy incorporated with a CCD camera.

2.3 *Drosophila Larva Analysis*

In the oenocyte experiment, the L3-larvae were chosen and placed on the moistened tissue paper for 0 (fed) or 16 h (starved). In the fat body experiment, the L2-larvae were chosen and placed on the moistened tissue paper for 0 (fed) or 48 h (starved). In the starvation assay, the L2-larvae were chosen and placed on the moistened tissue paper for 0 to 120 h. Their viability was determined by the pharynx movement every 12 h. Before *in vivo* observation, larvae were anesthetized by exposure to ether fume for 2 to 3 min. Temperature was kept at 22°C during observation.

2.4 *CARS/TPE-F Microscopy*

In the setup, one Ti-sapphire laser (Mira-900P, Coherent, California) with 2.5-ps pulse width serves as pump/probe beam, and the other Ti-sapphire laser (Mira-900F) with 200-fs pulse width serves as Stokes beam in CARS, both are at 76 MHz repetition rate (Fig. 1). Here the 200-fs pulsed Ti-sapphire laser can provide better efficiency of two-photon excitation of autofluorescence and green fluorescent protein (GFP). Both lasers are pumped by a Nd:YVO4 laser (Verdi-10W, Coherent, Santa Clara, California). An additional synchronization system (Synchro-Lock, Coherent, Santa Clara, California) is applied to synchronize the two laser pulses. The laser beams are collinearly combined and directed into a laser scanning microscope (FV300 and IX-71, Olympus, Tokyo, Japan), and focused onto the sample by a 60X N.A. = 1.2 water immersion objective (UPLSAPO 60XW, Olympus, Tokyo, Japan). To obtain CARS imaging of lipid C-H stretching mode at ~2845 cm^{-1}, the pump/probe beam is tuned at ~710 nm, and the Stocks beam is tuned at ~890 nm, with 30 and 15 mW at the sample, respectively. The forward CARS (F-CARS) signal (at ~590 nm)

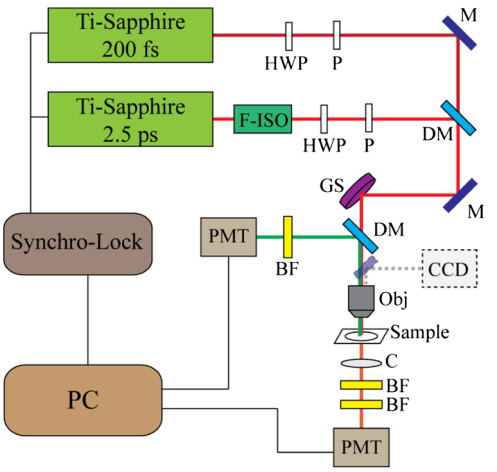

Fig. 1 Schematic Setup of CARS/TPE-F Microscope. F-ISO: Faraday isolator, BS: beam splitter, HWP: half-wave plate, P: polarizer, GS: galvo scanner, DM: dichroic mirror, BF: bandpass filter, C: condensor, Obj: objective.

is collected by a condenser (N.A. = 0.55), passing through a set of bandpass filters (FF01-630/92 and FF01-590/10, Semrock, Rochester, New York) and detected by a PMT (R7400U-02, Hamamatsu, Iwata-City, Japan). The TPE-F images are obtained simultaneously with CARS images. The fluorescence is collected by the same objective (epi-detection), passing through a short-pass dichroic mirror (685SPXR, Chroma, Bellows Falls, Vermont) and a bandpass filter (FF01-510/84, Semrock, New York), detected by a PMT (R3896, Hamamatsu, Japan). The scan speed is about 3 to 5 s for each CARS/TPE-F image. These images are shown as the overlay of CARS (pseudo-colored in yellowish orange) and TPE-F (pseudo-colored in green) images.

2.5 *Image Analysis of Lipid Content in Oenocytes and Fat Body*

For oenocytes, CARS/TPE-F images were focused on the plane, which showed clear contours of cell nuclei. LDs were identified from the thresholded CARS image and the CARS intensity of LDs was subtracted by the background, which is defined by nonlipid surrounding regions. The lipid content was determined by the square root of the background-subtracted CARS intensity,[33] and then multiplied by LDs area and divided by oenocytes area to give the normalized CARS intensity. On the other hand, for the fat body, we acquired images from several focal planes and estimated the lipid content by averaging the ratio of LDs area to the fat body area of these images. The area of the oenocyte and fat body was determined by the segmented TPE-F image. All image analyses were performed by Image-J. Statistical significance was calculated by using an unpaired two-tailed Student's t test. Error bars represent standard deviations.

3 Results and Discussion

3.1 *In Vivo Imaging of Drosophila Larvae by CARS/TPE-F Microscopy*

The larval oenocytes, clusters of pear-shaped cells, are found in the space between the dorsoventral muscles and the body wall.[45,46] Freshly dissected oenocytes often show greenish-yellow autofluorescence upon excitation with ultraviolet light, but it quenches rapidly.[45] Using CARS/TPE-F microscopy to observe the third-instar larva, we can recognize oenocytes by their cell morphology and autofluorescence [Fig. 2(b)]. The oenocytes are located at the basal surface of the lateral epidermis (at ~5 μm depth from the cuticle), in the presence of repetitive clusters on the side of the larval body [Fig. 2(a) and 2(b)]. CARS was tuned at ~2845 cm^{-1} corresponding with C-H bond stretching mode for lipid imaging. Figure 2(b) shows the CARS signal in oenocytes, indicating lipid accumulation. When we focus deeper at ~20 μm depth from the cuticle, we can also find the fat body and the gut, as shown in Fig. 2(c). The fat body has thin lobes composed of fat cells with large LDs and is clearly resolved by its strong CARS signal [Fig. 2(c)]. Some part of the gut shows autofluorescence (perhaps from the food) and has small LDs on it [Fig. 2(c)]. The larval cuticle also has strong autofluorescence that gives us clear contour of the larval body in CARS/TPE-F images [Fig. 2(b) and 2(c)]. This demonstrates that CARS/TPE-F microscopy can be used to visualize lipid distribution and autofluorescent organs in living *Drosophila* larva, with good axial and spatial resolution at subcellular level. This approach enables us to observe and monitor lipid dynamics in a noninvasive way.

To visualize the lipid in larval oenocytes and the fat body, we compared conventional bright-field images of Oil Red O stained tissues [Fig. 3(a) and 3(c)] with CARS/TPE-F images of a living larva [Fig. 3(b) and 3(d)]. When the larva is starved, its oenocytes will accumulate lipid-like liver steatosis in mammals,[7] shown as many Oil-Red-O-positive LDs in Fig. 3(a). In the *in vivo* CARS/TPE-F image [Fig. 3(b)], oenocytes are identified by their autofluorescence from the TPE-F signal (pseudo-colored in green) and accumulated LDs are also clearly resolved from the CARS signal (pseudo-colored in yellowish orange) [Fig. 3(b)]. Moreover, *in vivo* CARS/TPE-F image shows a better feature of each lipid droplet (LD) [Fig. 3(b)], while the image of Oil Red O stained tissue shows LDs as reddish fuzzy spots [Fig. 3(a)] due to possible aggregation caused by fixation and staining procedures.[47,48] In addition, from *in vivo* CARS/TPE-F image, we not only observe autofluorescence of oenocytes but also find some fluorescent globules in the cytoplasm (pseudo-colored in green) [Fig. 3(b)] which could be the protein granules,[49] providing us more information about its metabolic status.

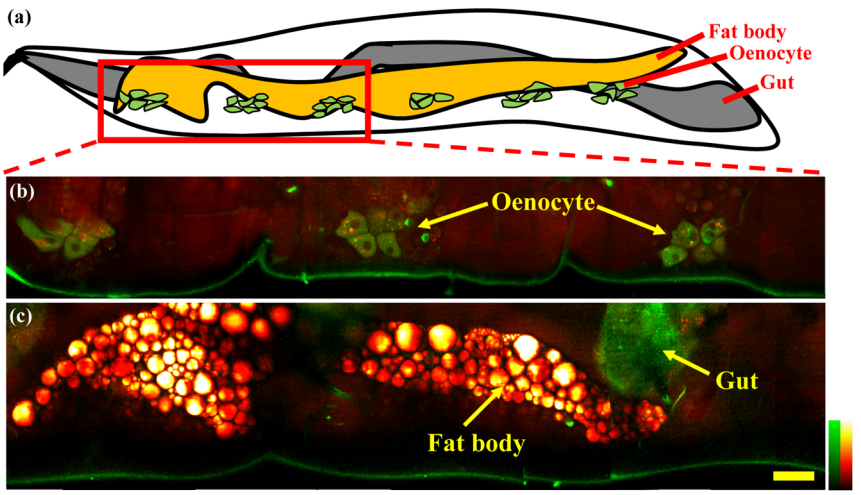

Fig. 2 The internal organs of a living *Drosophila* larva: (a) a schematic drawing of internal organs in a larva; (b) the CARS/TPE-F images of oenocytes in a larva, at depth = 5 μm from the cuticle; (c) the CARS/TPE-F images of the fat body and gut in a larva, at depth = 20 μm from the cuticle. Scale bar: 30 μm. (Yellowish orange: CARS, green: autofluorescence).

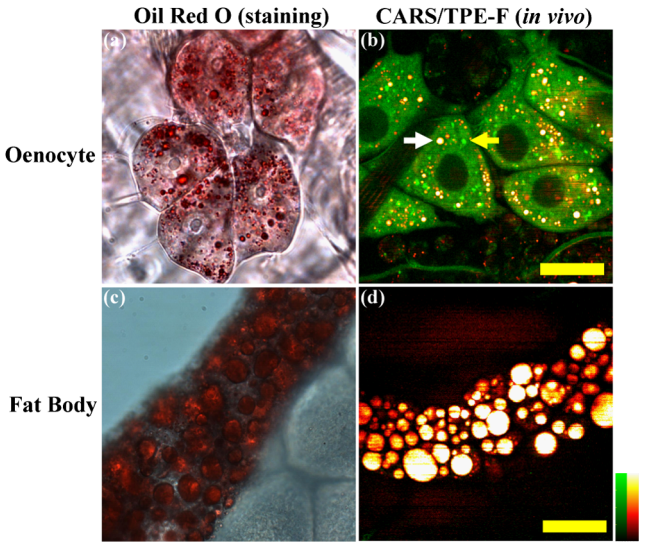

Fig. 3 Larval oenocytes and the fat body: (a) Oil Red O stained bright field and (b) *in vivo* CARS/TPE-F images of oenocytes. The lipid droplet and fluorescent globule are indicated by the white arrow and yellow arrow, respectively. Scale bar: 20 μm. (c) Oil Red O stained bright field and (d) *in vivo* CARS/TPE-F images of the fat body. Scale bar: 30 μm. (Yellowish orange: CARS, green: autofluorescence).

Likewise, compared with the image of Oil Red O stained tissue [Fig. 3(c)], *in vivo* CARS/TPE-F image shows better resolution of LDs and gives us the fine structure of the fat body [Fig. 3(d)]. Using fluorescent fusion proteins such as GFP can also achieve *in vivo* imaging of LDs in *Drosophila* fat body.[21] However, the fluorescent protein is labeled on a specific protein (such as PERILIPIN1 or Lsd-1) that expresses on the surface of LDs, and therefore its fluorescence cannot truly reflect the lipid content in LDs. Unlike fluorescent protein labeling, the CARS signal can be specific to C-H bonds mainly from neutral lipid in LDs. In conclusion, *in vivo* imaging via CARS/TPE-F microscopy can preserve the most natural information including the feature of LDs, the lipid content, and the autofluorescence.

3.2 *Lipid Regulation in Larval Oenocytes*

To investigate lipid regulation in larval oenocytes and fat body, each of two lipid regulatory proteins—Bmm or Lsd-2—was overexpressed in the fat body of *Drosophila* to observe their effects. The imbalance between these two proteins can alter lipid metabolism in *Drosophila*. Figure 4(a) through 4(f) are CARS/TPE-F images of oenocytes under fed and starved (16 h) conditions. In the control larva (w^{1118}), oenocytes normally do not accumulate much lipid under fed condition [Fig. 4(a)]. When it is starved, lipolysis (TAG hydrolysis) occurs in the fat body and the fatty acids are released from the fat body to oenocytes. As a result, more LDs accumulate in oenocytes ($N = 13$ larvae) [Fig. 4(b)].[7] However, in FB-Bmm-overexpressing mutant (FB-Gal4:UAS-Bmm), LDs accumulate in oenocytes even when it is fed [Fig. 4(c)][7] and accumulate more when starved ($N = 8$ larvae) [Fig. 4(d)]. On the contrary, in FB-Lsd-2-overexpressing mutant (FB-Gal4:UAS-Lsd-2), LDs are less found in oenocytes both under fed and starved conditions ($N = 12$ larvae) [Fig. 4(e) and 4(f)].[7] The image analysis of lipid content in oenocytes is shown in Fig. 4(g). FB-Bmm-overexpressing mutant has ~twofold more lipid than wild-type under fed condition, while FB-Lsd-2-overexpressing

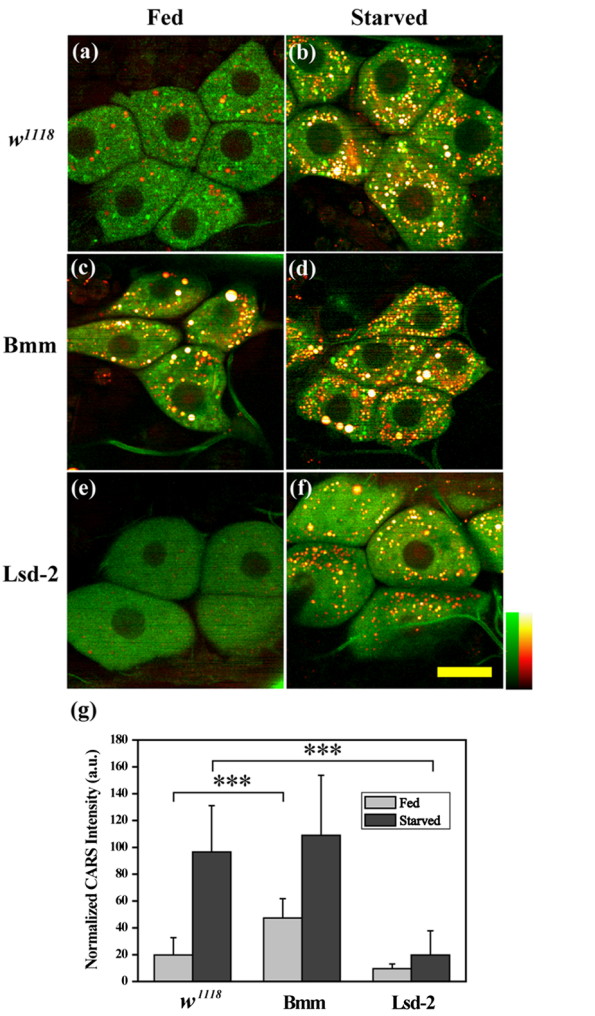

Fig. 4 The CARS/TPE-F images of oenocytes under fed and starved conditions, in the control (w^{1118}) [(a) and (b)], Bmm overexpression under the control of FB-Gal4 (Bmm) [(c) and (d)], and Lsd-2 overexpression under the control of FB-Gal4 (Lsd-2) [(e) and (f)]. Scale bar: 20 μm. (Yellowish orange: CARS, green: autofluorescence). (g) Analysis of lipid content in oenocytes under fed and starved conditions. (Error bars represent standard deviations of oenocytes from 8 to 13 larvae. $***p < 0.0001$.)

mutant has ~fourfold less lipid than wild-type under starved condition [Fig. 4(g)]. Grönke et al. have found that Bmm would be upregulated upon starvation in normal flies.[16] Thus, overexpression of Bmm in the fat body is likely to mimic the effect of starvation and lead to more LDs accumulation in oenocytes. On the other hand, Lsd-2 acts antagonistically to Bmm and hinders the access of Bmm to LDs,[9,16] thus can lower the lipolysis rate when overexpressed. Indeed, we found less accumulation of LDs in FB-Lsd-2-overexpressing mutant oenocytes even when starved. These results indicate that promotion and inhibition of TAG hydrolysis in the fat body can significantly perturb lipid metabolism in the larva under fed and starved condition.

3.3 *Lipid Regulation in the Fat Body*

We further investigated the effect of overexpression of Bmm and Lsd-2 on lipid regulation in larval fat body. Figure 5 shows CARS/TPE-F images of the fat body of FB-Gal4 [Fig. 5(a)

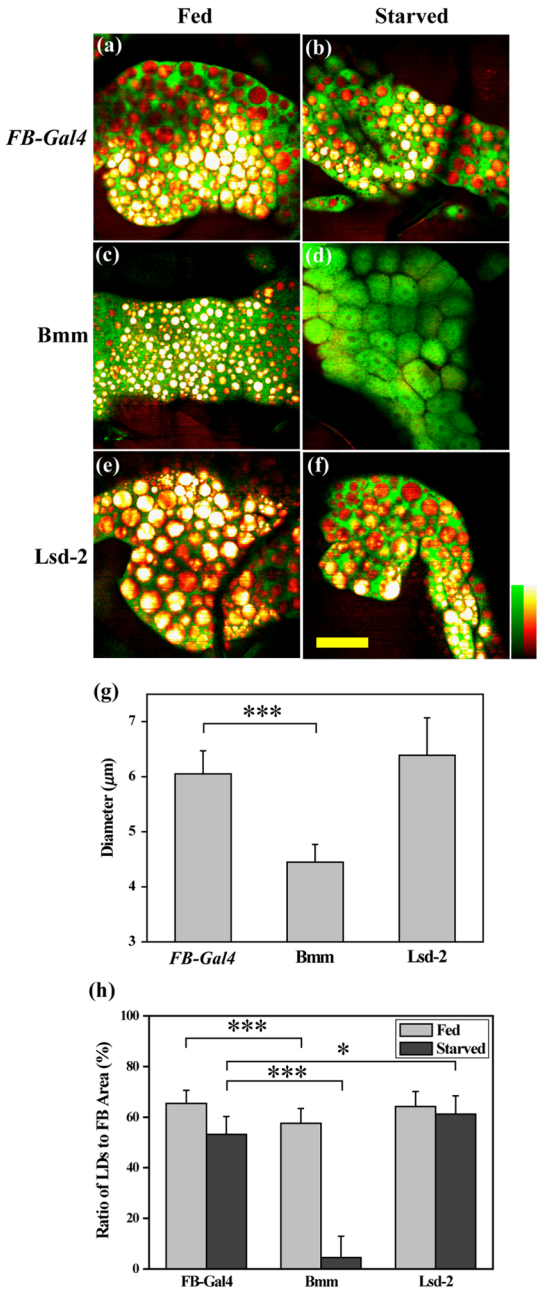

Fig. 5 The CARS/TPE-F images of the fat body under fed and starved conditions, in the control (FB-Gal4) [(a) and (b)], Bmm overexpression under the control of FB-Gal4 (Bmm) [(c) and (d)], and Lsd-2 overexpression under the control of FB-Gal4 (Lsd-2) [(e) and (f)]. Scale bar: 30 μm. (Yellowish orange: CARS, green: GFP) (g) Average LD size in the fat body. (Error bars represent standard deviations of 17 to 22 LDs for each mutant. $***p < 0.0001$.) (h) The ratio of LDs area to the fat body area of each larva under fed and starved conditions. (Error bars represent standard deviations of fat bodies from 8 ~ 11 larvae. $*p < 0.01$, $***p < 0.0001$.)

and 5(b)] (as control), FB-Bmm-overexpressing mutant [Fig. 5(c) and 5(d)], and FB-Lsd-2-overexpressing mutant [Fig. 5(e) and 5(f)] under fed and starved (48 h) conditions. Because these mutants are generated by the FB-Gal4 driver which expresses GFP in fat cells,[12] both mutants show GFP fluorescence in their fat bodies. Therefore we can identify the LDs by CARS signal (pseudo-colored in yellowish orange) in the region of the fat body by TPE-F signal (pseudo-colored in green). Under fed condition, the average size of LDs [Fig. 5(g)] in the fat body of FB-Bmm-overexpressing mutant is much smaller (~4.5 μm in diameter) ($N = 22$ LDs) [Fig. 5(c)] than that of the control larva (~6.1 μm in diameter) ($N = 17$ LDs) [Fig. 5(a)], whereas the size of LDs in the fat body of FB-Lsd-2-overexpressing mutant is slightly larger (~6.4 μm in diameter) ($N = 18$ LDs) [Fig. 5(e)]. Grönke et al. have found that overexpression of Bmm can reduce the size and number of LDs in fat cells of adult flies,[16] and overexpression of Lsd-2 can increase total TAG content of adult flies.[12] Our results demonstrate that they can have different sizes of LDs at larval stage, especially in FB-Bmm-overexpressing mutant. The reduced size of LDs in FB-Bmm-overexpressing mutant larval fat body implies that promotion of lipolysis decreases the formation of large LDs. We further analyzed the lipid content in their fat bodies. Unlike oenocytes, which locate near the surface (at ~5 μm depth), the fat body distributes more deeply (at ~20 μm depth) in the larval body, and the intensity of its CARS signal decays with the depth. To avoid the problem it may cause in lipid quantification, we used the density of LDs in the fat body (the ratio of LDs area to the fat body area) instead of the CARS intensity to estimate the lipid content [Fig. 5(h)]. We found that FB-Bmm-overexpressing mutant has lower lipid content under fed condition, and the lipid content dramatically decreases after 48 h starvation ($N = 10$ larvae) [Fig. 5(d)]. On the contrary, the lipid content in FB-Lsd-2-overexpressing mutant decreases less than in the control after starvation ($N = 8$ larvae) [Fig. 5(f)]. It was reported that LDs can aggregate under starvation.[50] However, we did not observe discernible LDs aggregation in the fat body [Fig. 5(b) and 5(f)]. Our results demonstrate that overexpression of Bmm can cause smaller LDs and lower lipid content in the larval fat body and faster consumption of lipid under starvation, while overexpression of Lsd-2 results in slower consumption of lipid under starvation.

To evaluate the correlation between the lipid metabolism and the viability under long-term food-deprived condition, we performed the starvation assay (0 to 120 h) on L2-larvae of w^{1118}, FB-Gal4, FB-Bmm-overexpressing mutant, and FB-Lsd-2-overexpressing mutant to measure their lifespans under starvation, as shown in Fig. 6. The mean lifespan of FB-Bmm-overexpressing mutant is 57.9 ± 2.9 h ($N = 40$), while that of FB-Lsd-2-overexpressing mutant is 87.3 ± 3.4 h

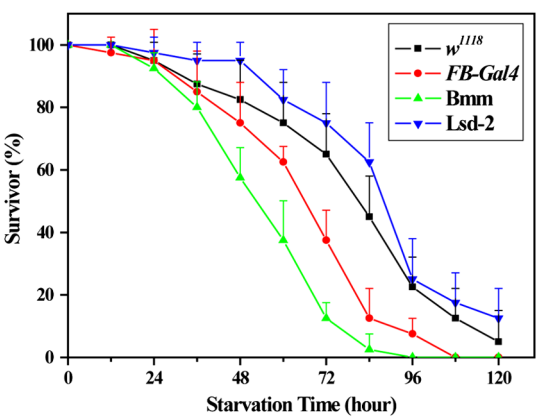

Fig. 6 Life span of w^{1118}, FB-Gal4, FB-Bmm-overexpressing mutant (Bmm), and FB-Lsd-2-overexpressing mutant (Lsd-2) under starvation. (Error bars represent standard deviations from total 40 larvae in four independent experiments.)

($N = 40$) and that of the control (FB-Gal4) is 68.7 ± 3.6 h ($N = 40$) (Fig. 6). FB-Bmm-overexpressing mutant has a shorter lifespan whereas FB-Lsd-2-overexpressing mutant has a longer lifespan with respect to the control. In summary, Bmm and Lsd-2 regulate lipid in an opposite way, and overexpression of these proteins can result in different sizes of LDs and rate of lipid consumption in the larval fat body, which can strongly affect their viability under starvation.

4 Conclusion

CARS/TPE-F microscopy provides *in vivo* imaging of lipid (from CARS signal) and identification of the oenocyte/fat body (from TPE-F signal), which allows us to monitor the lipid regulation in them at subcellular level. Overexpression of Bmm can cause abnormal LDs accumulation in oenocytes and smaller size of LDs in the fat body under fed condition, while overexpression of Lsd-2 inhibits LDs accumulation in oenocytes and slightly increases the size of LDs in the fat body. In addition, the viability during long-term starvation is correlated to the consumption of lipid. In FB-Bmm-overexpressing mutant, the higher rate of lipid consumption makes it more vulnerable to food-deprived condition, while in FB-Lsd-2-overexpressing mutant the lower rate of lipid consumption makes it more resistant to starvation. The similarity of the fat body and oenocytes of *Drosophila* to the adipose tissue and hepatocytes of human, with Bmm and Lsd-2 protein homologs to human ATGL and Perilipin/ADRP, suggests that the study of lipid homeostasis in *Drosophila* can provide useful information to our understanding of lipid metabolism in human and will possibly explore a way to tackle human metabolic diseases.

Acknowledgments

This work was supported by Academia Sinica and the National Science Council of the Republic of China (Grant No. NSC-98-2113-M001-025). We thank Dr. Ronald Kühnlein for FB-Gal4, UAS-Bmm, UAS-Lsd-2 strains, and for critical reading of the manuscript. We thank fly core facility in College of Medicine, National Taiwan University and sixth common core lab in National Taiwan University Hospital for experimental materials and technical support.

References

1. C. H. Lee, "Minireview: lipid metabolism, metabolic diseases, and peroxisome proliferator-activated receptors," *Endocrinology* **144**(6), 2201–2207 (2003).
2. J. Galgani and E. Ravussin, "Energy metabolism, fuel selection and body weight regulation," *Int. J. Obes. (Lond)* **32**, S109–S119 (2008).
3. R. P. Kühnlein, "*Drosophila* as a lipotoxicity model organism—more than a promise?," *Biochim. Biophys. Acta* **1801**(3), 215–221 (2010).
4. K. N. Bharucha, "The epicurean fly: using *Drosophila melanogaster* to study metabolism," *Pediatr. Res.* **65**(2), 132–137 (2009).
5. A. Schlegel and D. Y. R. Stainier, "Lessons from 'lower' organisms: what worms, flies, and zebrafish can teach us about human energy metabolism," *Plos Genet.* **3**(11), 2037–2048 (2007).
6. E. L. Arrese and J. L. Soulages, "Insect fat body: energy, metabolism, and regulation," *Annu. Rev. Entomol.* **55**(1), 207–225 (2010).
7. E. Gutierrez et al., "Specialized hepatocyte-like cells regulate *Drosophila* lipid metabolism," *Nature* **445**(7125), 275–280 (2007).
8. N. Arquier and P. Léopold, "Fly foie gras: modeling fatty liver in *Drosophila*," *Cell Metab.* **5**(2), 83–85 (2007).
9. P. E. Bickel, J. T. Tansey, and M. A. Welte, "PAT proteins, an ancient family of lipid droplet proteins that regulate cellular lipid stores," *Biochim. Biophys. Acta* **1791**(6), 419–440 (2009).
10. A. R. Kimmel et al., "Adoption of PERILIPIN as a unifying nomenclature for the mammalian PAT-family of intracellular lipid storage droplet proteins," *J. Lipid Res.* **51**(3), 468–471 (2010).
11. S. Miura et al., "Functional conservation for lipid storage droplet association among Perilipin, ADRP, and TIP47 (PAT)-related proteins in mammals, *Drosophila*, and Dictyostelium," *J. Biol. Chem.* **277**(35), 32253–32257 (2002).
12. S. Grönke et al., "Control of fat storage by a *Drosophila* PAT domain protein," *Curr. Biol.* **13**(7), 603–606 (2003).
13. L. Teixeira et al., "*Drosophila* Perilipin/ADRP homologue Lsd2 regulates lipid metabolism," *Mech. Dev.* **120**(9), 1071–1081 (2003).
14. R. P. Kühnlein, "The contribution of the *Drosophila* model to lipid droplet research," *Progr. Lipid Res.* **50**(4), 348–356 (2011).
15. J. Bi et al., "Opposite and redundant roles of the two *Drosophila* Perilipins in lipid mobilization," *J. Cell. Sci.* **125**, 3568–3577 (2012).
16. S. Grönke et al., "Brummer lipase is an evolutionary conserved fat storage regulator in *Drosophila*," *Cell Metab.* **1**(5), 323–330 (2005).
17. J. Spandl et al., "Live cell multicolor imaging of lipid droplets with a new dye, LD540," *Traffic* **10**(11), 1579–1584 (2009).
18. M. V. Ranall, B. G. Gabrielli, and T. J. Gonda, "High-content imaging of neutral lipid droplets with 1,6-diphenylhexatriene," *BioTechniques* **51**(1), 35–36, 38–42 (2011).
19. K. Brooks, B. Liang, and J. Watts, "The influence of bacterial diet on fat storage in *C. elegans*," *Plos One* **4**(10), e7545 (2009).
20. K. Yen et al., "A comparative study of fat storage quantitation in nematode caenorhabditis elegans using label and label-free methods," *Plos One* **5**(9), e12810 (2010).
21. M. Beller et al., "PERILIPIN-dependent control of lipid droplet structure and fat storage in *Drosophila*," *Cell Metab.* **12**(5), 521–532 (2010).
22. M. A. Welte et al., "Developmental regulation of vesicle transport in *Drosophila* embryos: forces and kinetics," *Cell* **92**(4), 547–557 (1998).
23. D. Débarre et al., "Imaging lipid bodies in cells and tissues using third-harmonic generation microscopy," *Nat. Methods* **3**(1), 47–53 (2006).
24. I. Gaspar and J. Szabad, "*In vivo* analysis of MT-based vesicle transport by confocal reflection microscopy," *Cell motility and the Cytoskeleton* **66**(2), 68–79 (2009).
25. C. H. Chien et al., "Label-free imaging of *Drosophila in vivo* by coherent anti-Stokes Raman scattering and two-photon excitation autofluorescence microscopy," *J. Biomed. Opt.* **16**(1), 016012 (2011).
26. H.-W. Wang et al., "Label-free bond-selective imaging by listening to vibrationally excited molecules," *Phys. Rev. Lett.* **106**(23), 238106 (2011).
27. T. T. Le, S. Yue, and J. X. Cheng, "Shedding new light on lipid biology with coherent anti-Stokes Raman scattering microscopy," *J. Lipid Res.* **51**(11), 3091–3102 (2010).
28. M. D. Duncan, J. Reintjes, and T. J. Manuccia, "Scanning coherent anti-Stokes Raman microscope," *Opt. Lett.* **7**(8), 350–352 (1982).
29. A. Zumbusch, G. R. Holtom, and X. S. Xie, "Three-dimensional vibrational imaging by coherent anti-Stokes Raman scattering," *Phys. Rev. Lett.* **82**(20), 4142–4145 (1999).
30. C. L. Evans et al., "Chemical imaging of tissue *in vivo* with video-rate coherent anti-Stokes Raman scattering microscopy," *Proc. Natl. Acad. Sci. U. S. A.* **102**(46), 16807–16812 (2005).
31. Y. Fu et al., "*Ex vivo* and *in vivo* imaging of myelin fibers in mouse brain by coherent anti-Stokes Raman scattering microscopy," *Opt. Express* **16**(24), 19396–19409 (2008).
32. E. Bélanger et al., "Quantitative myelin imaging with coherent anti-Stokes Raman scattering microscopy: alleviating the excitation polarization dependence with circularly polarized laser beams," *Opt. Express* **17**(21), 18419–18432 (2009).
33. Y. M. Wu et al., "Quantitative assessment of hepatic fat of intact liver tissues with coherent anti-stokes Raman scattering microscopy," *Anal. Chem.* **81**(4), 1496–1504 (2009).
34. J. Zhu et al., "A dynamic, cytoplasmic triacylglycerol pool in enterocytes revealed by *ex vivo* and *in vivo* coherent anti-Stokes Raman scattering imaging," *J. Lipid Res.* **50**(6), 1080–1089 (2009).
35. S. H. Kim et al., "Multiplex coherent anti-stokes Raman spectroscopy images intact atheromatous lesions and concomitantly identifies distinct chemical profiles of atherosclerotic lipids," *Circul. Res.* **106**(8), 1332–1341 (2010).

36. J. Lin et al., "Assessment of liver steatosis and fibrosis in rats using integrated coherent anti-Stokes Raman scattering and multiphoton imaging technique," *J. Biomed. Opt.* **16**(11), 116024 (2011).
37. C. Y. Lin et al., "Picosecond spectral coherent anti-Stokes Raman scattering imaging with principal component analysis of meibomian glands," *J. Biomed. Opt.* **16**(2), 021104 (2011).
38. M. Zimmerley et al., "Quantitative detection of chemical compounds in human hair with coherent anti-Stokes Raman scattering microscopy," *J. Biomed. Opt.* **14**(4), 044019 (2009).
39. K. König et al., "Optical skin biopsies by clinical CARS and multiphoton fluorescence/SHG tomography," *Laser Phys. Lett.* **8**(6), 465–468 (2011).
40. L. Gao et al., "On-the-spot lung cancer differential diagnosis by label-free, molecular vibrational imaging and knowledge-based classification," *J. Biomed. Opt.* **16**(9), 096004 (2011).
41. T. Hellerer et al., "Monitoring of lipid storage in *Caenorhabditis elegans* using coherent anti-Stokes Raman scattering (CARS) microscopy," *Proc. Natl. Acad. Sci. U. S. A.* **104**(37), 14658–14663 (2007).
42. M. C. Wang et al., "RNAi screening for fat regulatory genes with SRS microscopy," *Nat. Methods* **8**(2), 135–138 (2011).
43. A. Enejder, C. Brackmann, and F. Svedberg, "Coherent anti-Stokes Raman scattering microscopy of cellular lipid storage," *IEEE J. Sel. Top. Quant.* **16**(3), 506–515 (2010).
44. C. H. Chien et al., "*In vivo* monitoring specialized hepatocyte-like cells in *Drosophila* by coherent anti-Stokes Raman scattering (CARS) and two-photon excitation fluorescence (TPE-F) microscopy," *Proc. SPIE* **8226**, 822624 (2012).
45. T. M. Rizki, "The circulatory system and associated cells and tissues," in *The Genetics and Biology of Drosophila*, M. Ashburner and T. R. F. Wright, Eds., pp. 397–452, Academic, New York (1978).
46. D. Bodenstein, "The postembryonic development of *Drosophila*," in *Biology of Drosophila*, M. Demerec, Ed., pp. 275–367, John Wiley and Sons, New York (1950).
47. S. Fukumoto and T. Fujimoto, "Deformation of lipid droplets in fixed samples," *Histochem. Cell Biol.* **118**(5), 423–428 (2002).
48. X. Nan, J. X. Cheng, and X. S. Xie, "Vibrational imaging of lipid droplets in live fibroblast cells with coherent anti-Stokes Raman scattering microscopy," *J. Lipid Res.* **44**(11), 2202–2208 (2003).
49. T. M. Rizki, "Fat Body," in *The Genetics and Biology of Drosophila*, M. Ashburner and T. R. F. Wright, Eds., pp. 561–601, Academic, New York (1978).
50. H. B. Zhang et al., "Regulation of cellular growth by the *Drosophila* target of rapamycin dTOR," *Gene Dev.* **14**(21), 2712–2724 (2000).